NASA Technical Memorandum 86896

NASA-TM-86896 19850007416

Effect of Steady-State Temperature Distortion on Inlet Flow to a High-Bypass-Ratio Turbofan Engine

Ronald H. Soeder and Charles M. Mehalic
Lewis Research Center
Cleveland, Ohio

and

Kevin Stancik
Air Force Systems Command Liaison Office
Lewis Research Center
Cleveland, Ohio

January 1985

NASA

EFFECT OF STEADY-STATE TEMPERATURE DISTORTION ON INLET FLOW TO A HIGH-BYPASS-RATIO TURBOFAN ENGINE

Ronald H. Soeder and Charles M. Mehalic
National Aeronautics and Space Administration
Lewis Research Center
Cleveland, Ohio 44135

and

Kevin Stancik
Air Force Systems Command Liaison Office
Lewis Research Center
Cleveland, Ohio 44135

E-2369

SUMMARY

The results of an investigation to determine the characteristics of steady-state temperature distortion with a high-bypass-ratio turbofan engine are reported herein. Flow angle, static and total pressure, and total temperature were measured between a rotatable hydrogen-fueled burner and the fan inlet. Fan and compressor characteristics were determined by measuring static and total pressure and total temperature at the fan exit and at the compressor inlet and exit. Static pressure measurements were also made in the passage upstream of the compressor inlet and at each stator stage inside the compressor.

The hydrogen burner, capable of ±30° rotation from top dead center, produced the various total temperature distortion intensities and orientations. Experiments were conducted with fan speeds (corrected to the undistorted temperature sectors at station 1) of 80 and 90 percent of rated (i.e., 7005 rpm) and Reynolds number indices of 0.3 and 0.5. Two temperatures distortion extents of 90° and 180° were evaluated.

Free-stream yaw flow angle increased between burner discharge and the fan inlet. The largest variation occurred in the hub region. Yaw flow angle did not vary with changes in corrected fan speed or Reynolds number index. Increasing the temperature distortion extent from 90° to 180° slightly increased yaw flow angle amplitude (by 1.6°).

Along the inlet duct wall the magnitude of the static pressure distortion increased exponentially as the flow approached the engine inlet. The total and static pressure profiles at the engine inlet and the compressor exit were flat, indicating that temperature distortion at these locations had no effect. The total temperature profile at the engine inlet was a square wave; it became sinusoidal at the compressor exit but remained the same intensity. This indicated that temperature distortion was not attenuated throughout the fan and compressor. Static pressure distortion increased through the first three stages of the compressor and remained constant at 10.5 percent until the ninth stage. The distortion then decreased through the remainder of the compressor to a level of 2.5 percent at the thirteenth stator stage.

INTRODUCTION

Analytical effort has been directed toward the development of low-bypass-ratio turbofan compressor models (refs. 1 to 3). Validation of these models required accurate measurement of the flow field at the engine inlet and throughout the compression system in the presence of temperature distortion and combined temperature and pressure distortion. Low-bypass-ratio engine investigations dealing with such distortions at the engine inlet are reported in references 4 to 8.

This investigation experimentally evaluated the effects of temperature distortions of different extents and intensities on a high-bypass-ratio turbofan engine. The effect of inlet pressure distortion on the same turbofan engine is presented in reference 9. The experimental data base obtained from these investigations will be used for model verification.

To evaluate inlet temperature distortion effects, total pressure, static pressure, and total temperature were surveyed at the engine inlet, the fan exit, and the compressor inlet and exit. Free-stream yaw flow angles were measured at two axial stations between the hydrogen burner and the fan inlet. Boundary-layer flow angles were also measured at the engine inlet. Static pressures were measured along the inlet duct wall to determine the level of inlet static pressure distortion. The expected static pressure variation upstream of an engine inlet is discussed in reference 10. Additional static pressure measurements were made at each of 13 stator stages inside the axial-flow compressor. Data are presented for two corrected fan speeds of 80 and 90 percent of rated condition (7005 rpm) at Reynolds number indices (RNI) of 0.3 and 0.5 (based on the undistorted sectors at the inlet flow measurement station). Total temperature distortion levels of 9.75 percent with 90°-extent distortion and 10.5 percent with 180°-extent distortion at the engine inlet were investigated.

SYMBOLS

NFR2 fan speed corrected to station 2 test conditions, $N_F/\sqrt{\theta_2}$, rpm

P pressure, Pa

PNFR2 fan speed corrected to station 2 test conditions as a percent of 7005 rpm

RNI Reynolds number index, $\delta/(\mu/\mu_{SLS})\sqrt{\theta}$

r_m mean radius of inlet duct, 0.56 m

T temperature, K

U tangential velocity, m/s

V axial velocity, m/s

x axial length, m

ß yaw angle, deg

Δ maximum-minimum difference

δ ratio of total pressure to standard sea-level static pressure

θ ratio of total temperature to standard sea-level static temperature

μ absolute viscosity, kg/(m s)

Subscripts:

av average

max maximum

min minimum

s static condition

sls standard sea-level static condition

T total condition

Stations:

1 airflow measurement station, located 126.64 cm upstream of engine inlet

1B yaw measurement station, located 57.62 cm upstream of engine inlet

1C end of static pressure taps along inlet duct wall, located 56.49 cm upstream of engine inlet

2 fan inlet pressure, temperature, and flow angle measurements, located 14.96 cm upstream of engine inlet

2A start of static pressure taps along inlet duct wall, located 3.81 cm upstream of engine inlet

2C compressor inlet: outer wall of passage located 57.91 cm downstream of engine inlet; inner wall of passage located 55.93 cm downstream of engine inlet

2D first-stage compressor stators

2E second-stage compressor stators

2F third-stage compressor stators

2G fourth-stage compressor stators

2H fifth-stage compressor stators

2I sixth-stage compressor stators

2J seventh-stage compressor stators

2K eighth-stage compressor stators

2L ninth-stage compressor stators

2M tenth-stage compressor stators

2N eleventh-stage compressor stators

2P twelfth-stage compressor stators

2R thirteenth-stage compressor stators

2.4 fan exit, located 30.80 cm downstream of engine inlet

2.5 inlet to gooseneck passage: outer wall of passage located 40.30 cm downstream of engine inlet; inner wall of passage located 37.25 cm downstream of engine inlet

2.6 gooseneck passage: outer wall of passage located 46.88 cm downstream of engine inlet; inner wall of passage located 43.42 cm downstream of engine inlet

2.7 gooseneck passage: outer wall of passage located 46.88 cm downstream of engine inlet; inner wall of passage located 43.42 cm downstream of engine inlet

3 compressor exit, located 121.23 cm downstream of engine inlet

APPARATUS

Engine

The engine used for this investigation was a YTF34 high-bypass-ratio (6.23) turbofan engine. A single-stage fan, with a compression ratio of 1.51, was driven by a four-stage low-pressure turbine. The 14-stage axial-flow compressor with a compression ratio of 14.5 was driven by a two-stage, air-cooled high-pressure turbine. The engine was installed in an altitude test chamber (fig. 1). An engine schematic and instrumentation station diagrams of the region upstream of the engine inlet, the fan exit, the compressor inlet, the interstage, and the compressor exit are shown in figure 2.

Distortion Device

A gaseous hydrogen burner used to produce steady-state temperature distortion at the engine inlet was installed upstream of the inlet duct bellmouth (fig. 3). The burner was capable of ±30° rotation from the center position and was divided into four individually controlled quadrants. Air passing through the burner was heated in selected 90° sectors. Each 90° burner sector contained six swirl-can pilot burners to provide the ignition source for the hydrogen. Also each 90° sector contained six annular gutters supported by one radial gutter and six circular tube manifolds (one inside each annular gutter) with small holes for hydrogen injection. A hydrogen manifold located outside the burner was connected to the six circular tube manifolds in each 90° sector by tubing and a flow-control valve. Hydrogen was supplied to the manifold by

additional tubing and a main flow-control valve. The burner was located 3.81 m (150 in) upstream of the engine inlet.

Instrumentation

Inlet duct and engine instrumentation is outlined schematically in figures 2 and 4 to 6. Total and static pressures were recorded by using Scanivalves. These measurements included pressure levels at the airflow-measuring station in the inlet duct (station 1; fig. 2); at the upstream flow-angle-measuring station (station 1B); along the inlet duct; and at the fan inlet, the fan exit, the compressor inlet, the interstage, and the compressor exit. Temperatures were measured at each station by using Chromel-Alumel thermocouples except at the fan duct (station 2.4), where copper-constantan thermocouples were used. All thermocouples were referenced to a 339 K (610 °R) oven, and Mach number recovery corrections were applied as discussed in reference 11.

The details of the free-stream and boundary-layer rakes for measuring yaw flow angles are shown in figures 5 and 6. Yaw angle is positive when the tangential flow component is in the direction of fan rotation (velocity triangle in figs. 5 and 6). A flow-angle-measuring rake was also located at station 1B. Flow angle probes were calibrated for a range of ±30° at the same free-stream Mach numbers encountered during engine experiments. The estimated error is ±1/2°. Additional information on flow angle probes can be found in reference 12.

Procedure

The hydrogen burner was used to produce steady-state temperature distortion at the engine inlet. A typical 180°-extent temperature distortion pattern was generated by igniting two adjacent hydrogen burner quadrants and increasing gaseous hydrogen flow until a predetermined average temperature of 319 K (575 °R) was achieved at the fan inlet. The circumferential profiles were generated by rotating the pattern past the instrumentation in 12 steps, with four sequential pairs of quadrants at each ±30° and 0° burner position. The same procedure was used for the 90°-extent temperature distortion tests. The average temperature over the distorted sector for these tests was also 319 K (575 °R). All pressure and temperature data were normalized to upstream plenum pressure and temperature to compensate for minor run-to-run variations.

For each static tap along the inlet duct wall (fig. 4), the maximum and minimum static pressures were identified for the profile generated by the test series of 12 data points. The difference between the maximum and minimum readings was normalized to a similar difference in the static pressure taps nearest the engine inlet (station 2A, fig. 4) and presented as a relative static pressure distortion level.

A consistent Reynolds number index (RNI) was achieved by maintaining approximately a 289 K (520 °R) total temperature in the undistorted sectors of the burner and adjusting inlet total pressure to obtain values of 0.30 or 0.50 at station 1. Fan mechanical speed was adjusted during steady-state temperature distortion investigations in order that corrected fan speed based on the undistorted burner sectors would result in speeds of 80 and 90 percent of rated (7005 rpm).

RESULTS

The effects of steady-state temperature distortion were investigated for 90°- and 180°-extent temperature distortions of 9.75- and 10.5-percent magnitude, respectively. The Reynolds number index at station 1 was maintained at 0.3 and 0.5 for corrected, undistorted fan speeds of 80 and 90 percent of rated condition. The effects of steady-state temperature distortion orientation on inlet flow angle, inlet duct static pressure variation, and fan and compressor performance are presented.

Yaw Flow Angle

Clean inlet. - The undistorted, streamline yaw flow angles 57.62 cm upstream of the engine inlet (station 1B) varied from -1.6° at the hub region to -2.5° at the tip region (fig. 7). The free-stream yaw flow angle at the fan inlet (station 2) varied from +0.1° at the hub to -2.8° at the tip region (fig. 8(a)). The tip, boundary-layer yaw flow angle at station 2 remained constant at +0.8° (fig. 8(b)).

Effect of distortion extent. - Yaw flow angle data were obtained at stations 1B and 2 at 90-percent corrected fan speed and 180°-extent temperature distortion with RNI equal to 0.5. At station 1B the yaw flow angle varied with relative circumferential position within a narrow data band of +0.2° to -0.7° (fig. 9). This nearly constant yaw flow angle at station 1B indicates that there are no cross flows of burned hydrogen gas at the burner exit.

At station 2 the largest variation in free-stream yaw flow angle occurred in the hub region (fig. 10(c)). The amplitude of the hub yaw flow angle at the fan inlet was $\pm$ 2°. Comparing this result with that presented in reference 9 shows that pressure distortion has a much greater effect on yaw flow angle variation than does temperature distortion. The magnitude of total temperature distortion at station 2 is defined as

$$\frac{T_{T,max} - T_{T,min}}{T_{T,av}} \tag{1}$$

The maximum and minimum values in this expression refer to rake-average values. The average temperature term refers to a face-average value.

Temperature distortion extent did influence the circumferential distribution and the peak-to-peak magnitude of the yaw flow angle at station 2 (fig. 11). For 90° and 180° distortion extents the largest peak-to-peak hub yaw flow angles were 1.9° and 3.5°, respectively. There was no noticeable difference in peak-to-peak amplitude between free-stream tip and boundary-layer tip regions (figs. 11(a) and (d)).

Effects of speed and Reynolds number index. - The two corrected fan speeds and two Reynolds number indices investigated had no effect on inlet free-stream yaw flow angle variation (figs. 12 and 13). The largest variation occurred in the hub region, and the amplitudes in the free-stream tip region and the boundary-layer region were similar. These data were recorded with 180°-extent, 10.5-percent temperature distortion at the fan inlet (station 2).

Static Pressure Distortion

Static pressure distortion change along the inlet duct wall from stations 1B to 2A (fig. 4) was investigated as a function of corrected fan speed, RNI, and temperature distortion extent (figs. 14 to 16). The static pressure distortion change developed in reference 10 and presented in references 6 and 7 for a low-bypass-ratio turbofan and in references 9 and 13 for a high-bypass-ratio turbofan was found to be applicable for this investigation. The distortion change is defined as $P_{s,max} - P_{s,min}$ for each location, normalized by $P_{s,max} - P_{s,min}$ at station 2A or $(\Delta P_s)/(\Delta P_s)_{2A}$. The theoretical curves presented in the figures can be mathematically expressed as

$$\frac{\Delta P_s}{(\Delta P_s)_{2A}} = \exp\left[\frac{-(x - x_{2A})}{r_m}\right] \tag{2}$$

The data presented in figures 14 to 16 were obtained from static pressure taps located at 235°. Similar results were obtained from taps located at 55°. These data show that the relative static pressure distortion does follow the exponential curve presented in reference 10. The normalized distance parameter x/r_m is the axial distance divided by the mean radius of the inlet duct. The data diverge from the exponential curve for $x/r_m > 0.76$. This divergence can be attributed to the yaw angle rake (station 1B) blocking inlet flow. In addition, the exponential relationship presented in equation (2) is based on a constant-area duct and frictionless flow, neither of which were present in these experiments. The conical spinner mounted on the front of the engine caused an area change to occur before the streamlines entered the fan inlet.

Inlet Pressure and Temperature

Profiles of the circumferential variation of free-stream, rake-average total pressure at stations 1B and 2 (fig. 17(a)) were flat. This indicates that total pressure distortion did not occur along the inlet duct or at the fan inlet. Profiles of the circumferential variation of rake-average total temperature at the airflow-measuring station (station 1) and station 2 were square waves and showed little change in amplitude along the inlet duct (fig. 17(b)).

The data presented in figures 17 to 29 were recorded with a 180°-extent temperature distortion of 10.5 percent at the fan inlet (station 2). The fan speed was 90 percent of rated (7005 rpm), and RNI in the undistorted sectors of station 1 was maintained at 0.5. These conditions prevailed unless otherwise noted.

Profiles of corrected fan speed and Reynolds number index (figs. 18 to 19) showed a square wave at the fan inlet and no change in amplitude with fan speed or RNI. The effect of distortion extent on total temperature variation at the fan inlet (fig. 20) was to vary the relative profile amplitude about the profile average value for distortion extents of 90° and 180°. The profile amplitude varied from 0.975 to 1.075 for the former and from 0.95 to 1.055 for the latter.

Compression System Pressure and Temperature

Effects of fan speed. - The effect of fan speed on normalized total pressure, total temperature and static pressure profiles was determined at the fan exit (station 2.4), the compressor inlet (station 2C), and the compressor exit (station 3) (fig. 21). Changing corrected fan speed from 80 to 90 percent of rated (7005 rpm) did not change the amplitude of these profiles across the compression system.

The total pressure distortion at station 2.4 was 3.5 percent. This level of total pressure distortion was produced in the fan by the temperature distortion. Total pressure distortion decreased from 3 percent at the compressor inlet (station 2C, fig. 21(d)) to 2 percent at the compressor exit (station 3, fig. 21(g)). The static pressure profiles were flat at the fan exit and at the compressor inlet and exit (figs. 21(b), (e), and (h)). The uniformity of the static pressure profiles was due to the lack of walls or other means of generating or maintaining a static pressure gradient.

Comparing the total temperature profiles at stations 2.4, 2C, and 3 (figs. 21(c), (f), and (i)) with the temperature profile at station 2 (fig. 18) revealed two important results. First, the 180°-extent temperature distortion present at the fan inlet (station 2) was maintained throughout the fan and compressor. Second, the fan and compressor temperature profiles shifted in the direction of engine rotation (clockwise) with respect to the station 2 profile. The profile shift at the fan exit (station 2.4) was 16.5°; at the compressor inlet (station 2C) it was 37.5°; and at the compressor exit (station 3) it was 171°. The temperature profile rotation was the result of temperature passing through a fan or compressor along a particle path (a property of state). The temperature distortion magnitude defined by equation (1) was calculated to be 10.5 percent at the fan inlet and remained at essentially that level through the fan and compressor.

Effects of RNI. - The effect of RNI on normalized total pressure, total temperature, and static pressure profiles was determined at the fan exit (station 2.4), the compressor inlet (station 2C), and the compressor exit (station 3) (fig. 22). Changing RNI at the engine inlet from 0.3 to 0.5 had no effect on the amplitude of these profiles across the compression system.

At all three stations (figs. 22(a), (d), and (g)) the total pressure distortion decreased from 3.5 percent at the fan exit to 2 percent at the compressor exit. The static pressure profiles (figs. 22(b), (e), and (h)) were unaffected by temperature distortion.

The 180°-extent temperature distortion present at the engine inlet was maintained throughout the compression system (figs. 22(c), (f), and (i)). Fan and compressor temperature profiles shifted in the direction of fan and compressor rotation with respect to the station 2 profiles. The profile shift at the fan exit (station 2.4), the compressor inlet (station 2C), and the compressor exit (station 3) was the same as noted in the discussion of figure 21.

Effects of temperature distortion extent. - The effects of temperature distortion extent on normalized total pressure, static pressure, and total temperature profiles were determined at the fan exit (station 2.4) and the compressor inlet (station 2C) and outlet (station 3) (fig. 23). The sinusoidal variation in the total pressure profiles (figs. 23(a), (d), and (g)) and the

flat static pressure profiles (figs. 23(b), (e), and (h)) were the same as discussed in conjunction with figures 21 and 22.

Distortion extent did influence the angular rotation of the temperature distortion (figs. 23(c), (f), and (i)). The fan and compressor profiles rotated with respect to fan inlet (station 2) profiles, for 90°- and 180°-extent distortion at station 2, as follows: 16.5° at the fan exit (station 2.4) for both distortion extents; 21° and 37.5°, respectively, at the compressor inlet (station 2C); and 157.5° and 171°, respectively at the compressor exit (station 3).

Static pressure profiles in passage upstream of compressor inlet. - The effects of changes in corrected fan speed, RNI, and distortion extent at the fan inlet on static pressure were determined (figs. 24 to 26). The nearly flat static pressure profiles at stations 2.5, 2.6, and 2.7 indicate a minimal amount of static pressure distortion along the compressor inlet passage.

Static pressure profiles inside compressor. - Compressor-stage static pressure profiles were determined from the first-stage stators (station 2D) to the thirteenth-stage stators (station 2R) (figs. 27 to 29). Only the odd-numbered stator stages inside the compressor are presented, but results were similar for the even-numbered compressor stages for the engine inlet variations that were investigated.

Changing corrected fan speed from 80 to 90 percent or varying RNI at the engine inlet from 0.3 to 0.5 had no effect on the amplitude of the static pressure distortion associated with any compressor stator stages. The overall static pressure profile amplitude (peak to peak) increased between the first-stage stators (station 2D) and the third-stage stators (station 2F). This can be verified by comparing figures 27(a) and (b) and figures 28(a) and (b). The profile amplitude of the low-pressure region (data below 1.0) increased between the first- and third-stage stators because of the temperature distortion entering the compressor inlet. The profile amplitude (peak to peak) remained constant between the third-stage stators and the seventh-stage stators (station 2J). This can be verified by comparing figures 27(b) and (d) and figures 28(b) and (d). The profile amplitude started to decrease in the ninth-stage stators (station 2L) but became flat for the thirteenth-stage stators (figs. 27(g) and 28(g)). This flatness indicates that the open exit of the compressor is controlling this pressure field in spite of the stator blades.

Changing the temperature distortion extent at the fan inlet from 90° to 180° influenced both the static pressure distortion extent and its circumferential location at various stator stages within the compressor (fig. 29). Sinusoidal static pressure profiles were determined from the first-stage stators through the ninth-stage stators (figs. 29(a) to (e)). The low-pressure-region static pressure amplitude (data below 1.0) increased between the first and third stator stages because of the temperature distortion entering the compressor inlet. The profile amplitude remained constant through the seventh stator stage (station 2J; fig. 29(d)) and then began to decrease through the remaining compressor stages. This decrease was caused by the compressor open exit as noted in the discussion of figures 27 and 28.

The 90°-extent temperature distortion at station 2 resulted in a 96° static pressure distortion extent at the first-stage stators (fig. 29(a)). The apparent increase in distortion extent to 120° from the third to the ninth

stator stages (figs. 29(b) to (e)) was the result of having a limited number of static pressure taps at each compressor-stator stage and the consequent difficulty in precisely defining the slope of the static pressure data from the distorted region (data below 1.0) to the undistorted region (data above 1.0). This problem was not experienced with static pressure data obtained from 180°-extent temperature distortion experiments as these data had a more gradual slope.

SUMMARY OF RESULTS

A YTF34 high-bypass-ratio turbofan engine was tested with 90°- and 180°-extent inlet temperature distortion. The results of this investigation are as follows:

1. Yaw flow angle and static pressure distortion increased along the inlet duct as airflow approached the engine inlet.

2. There was little or no change in total temperature distortion between the burner exit and the fan inlet.

3. There was no significant total pressure distortion along the inlet duct between the hydrogen burner and the engine inlet.

4. Static pressure distortion was generated in the compressor rotors by the temperature distortion. The change in static pressure distortion was usually greatest in the front stages of the compressor.

5. Total temperature distortion profiles tended to change from a square profile to a sinusoidal profile as the distortion passed through the compressor.

REFERENCES

1. Mazzawy, R.S.: Multiple Segment Parallel Compressor Model for Circumferential Flow Distortion. J. Eng. Power, vol. 99, no. 2, Apr. 1977, pp. 288-296.

2. Mazzawy, R.S.; and Banks, G.A.: Modeling and Analysis of the TF30-P-3 Compressor System with Inlet Pressure Distortion. (PWA-5302, Pratt & Whitney Aircraft; NASA Contract NAS3-18535.) NASA CR-134996, 1976.

3. Mazzawy, R.S.; and Banks, G.A.: Circumferential Distortion Modeling of the TF30-P-3 Compression System. (PWA-5448, Pratt & Whitney Aircraft; NASA Contract NAS3-18535.) NASA CR-135124, 1977.

4. Braithwaite, Willis M.: Experimental Evaluation of a TF30-P-3 Turbofan Engine in an Altitude Facility: Effect of Steady-State Temperature Distortion. NASA TM X-2921, 1973.

5. Abdelwahab, Mahmood: Effects of Temperature Transients at Fan Inlet of a Turbofan Engine. NASA TP-1031, 1977.

6. Soeder, Ronald H.; and Bobula, George A.: Effect of Steady-State Temperature Distortion and Combined Distortion on Inlet Flow to a Turbofan Engine. NASA TM-79237, 1979.

7. Braithwaite, W.M.; and Soeder, Ronald H.: Combined Pressure and Temperature Distortion Effects on Internal Flow of a Turbofan Engine. AIAA Paper 79-1309, June 1979.

8. Abdelwahab, Mahmood: Effects of Fan Inlet Temperature Disturbances on the Stability of a Turbofan Engine. NASA TM-82699, 1981.

9. Soeder, Ronald H.; and Bobula, George A.: Effect of Steady-State Pressure Distortion on Inlet Flow to a High-Bypass-Ratio Turbofan Engine. NASA TM-82964, 1982.

10. Plourde, G.A.; and Stenning, A.H.: Attenuation of Circumferential Inlet Distortion in Multistage Axial Compressors. J. Aircr., vol. 5, no. 3, May-June 1968, pp. 236-242.

11. Glawe, George E.; Simmons, Frederick S.; and Stickney, Truman M.: Radiation and Recovery Corrections and Time Constants of Several Chromel-Alumel Thermocouple Probes in High-Temperature, High-Velocity Gas Streams. NACA TN-3766, 1956.

12. Dudzinski, T.J.; and Krause, L.N.: Flow-Direction Measurement with Fixed-Position Probes. NASA TM X-1904, 1969.

13. Soeder, Ronald H.; and Mehalic, Charles M.: Effect of Combined Pressure and Temperature Distortion Orientation on High-Bypass-Ratio Turbofan Engine Stability. NASA TM-83771, 1984.

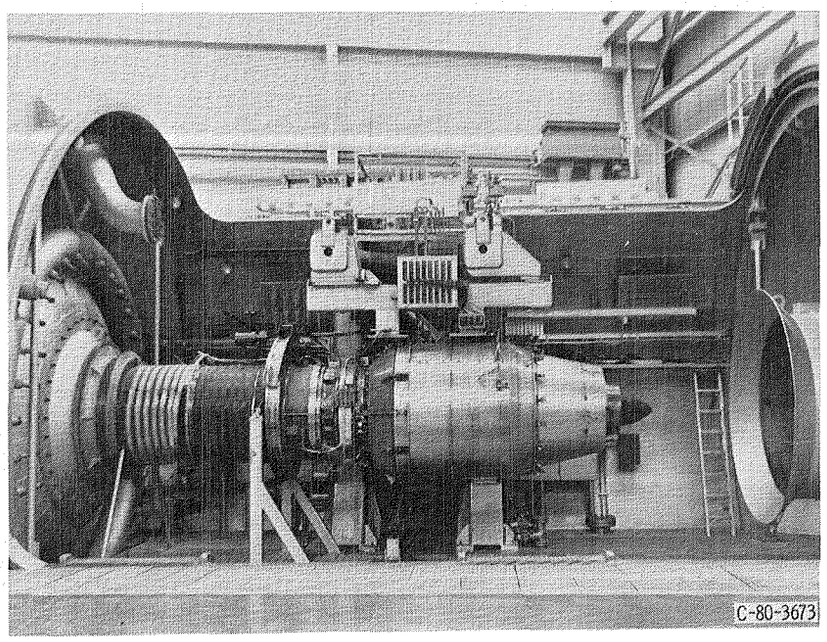

Figure 1. - YTF34 engine in altitude test chamber.

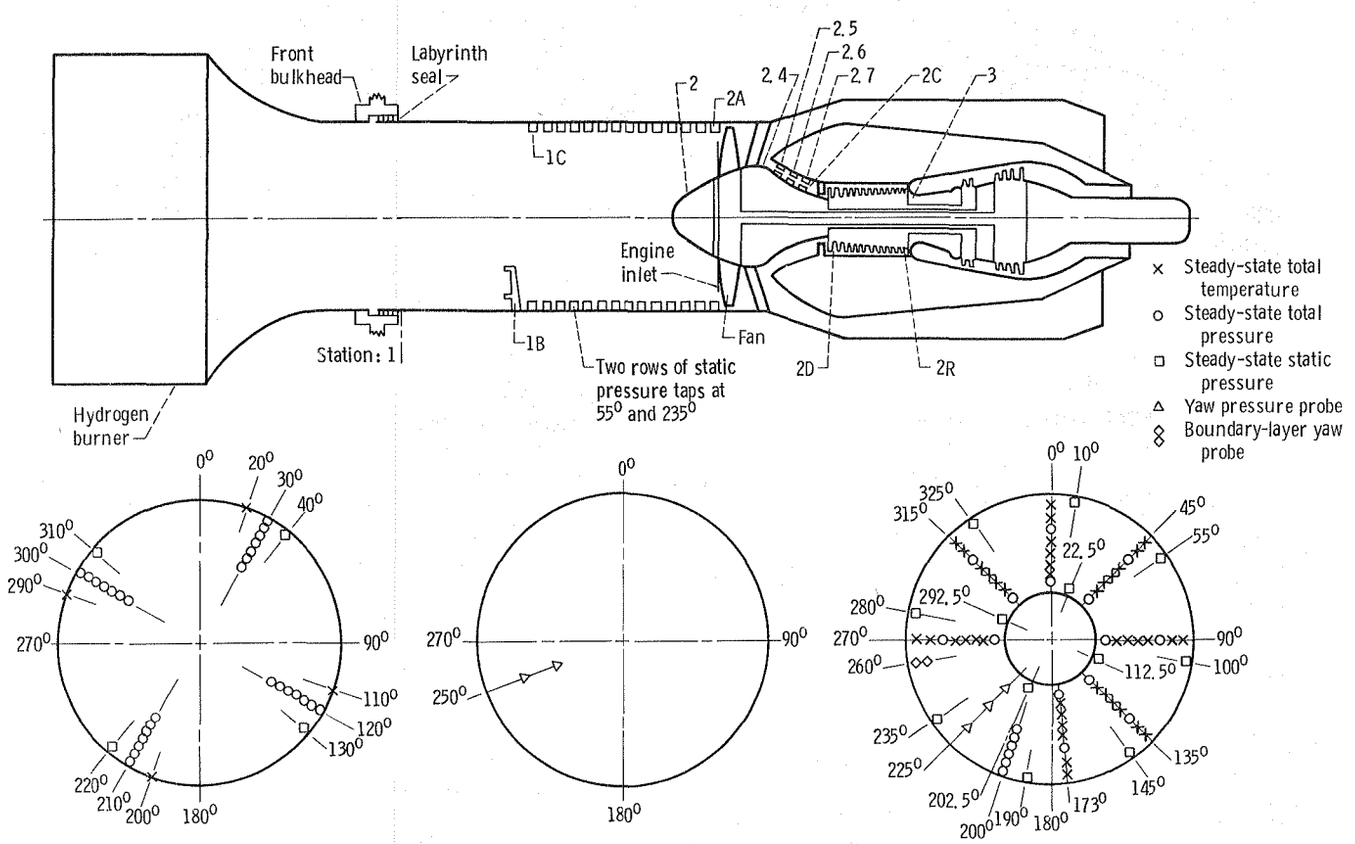

Station 1 (Airflow-metering station, 126.64 cm (49.86 in) upstream of engine inlet)

Station 1B (behind rotating screen assembly, 57.62 cm (22.69 in) upstream of engine inlet)

Station 2 (fan inlet, 14.96 cm (5.89 in) upstream of engine inlet)

Figure 2. - Instrumentation layout for YTF34 turbofan engine (stations viewed looking upstream).

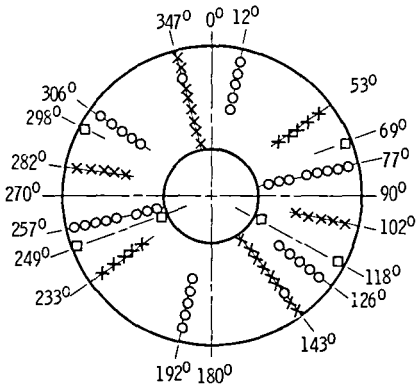

Station 2.4 (fan exit)

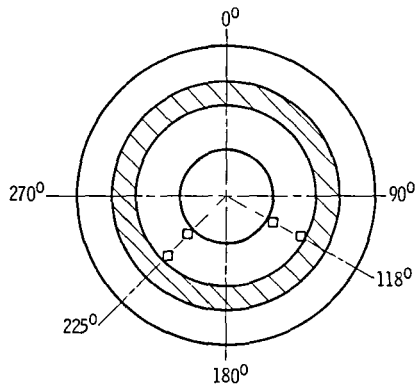

Stations 2.5, 2.6, and 2.7 (compressor flow passage)

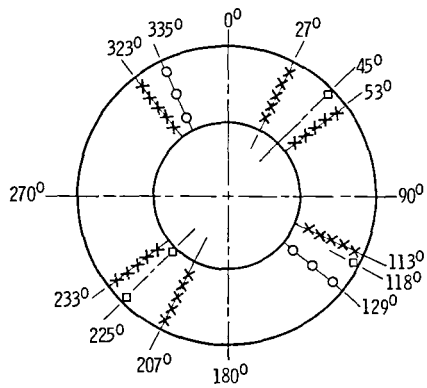

Station 2C (compressor inlet)

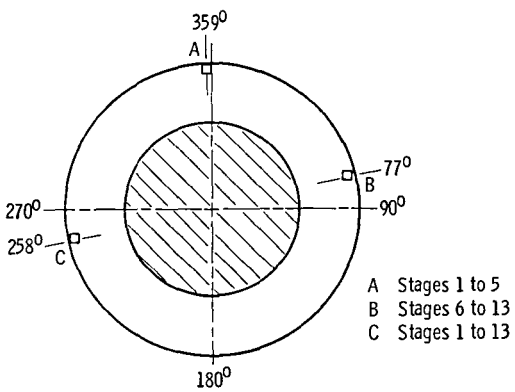

Stations 2D to 2R (compressor interstages)

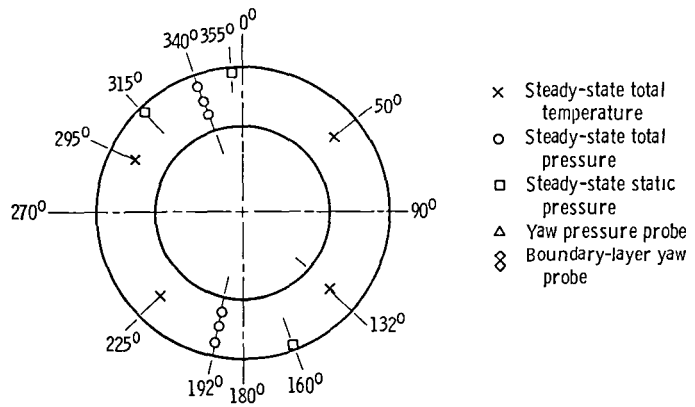

Station 3 (compressor exit)

Figure 2 - Concluded.

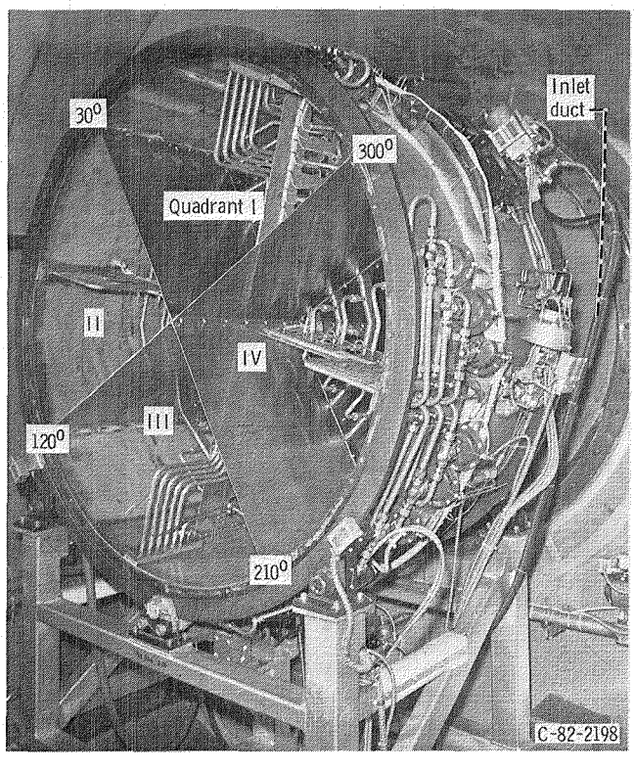

Figure 3. - Gaseous-hydrogen-fueled burner viewed in direction of engine inlet.

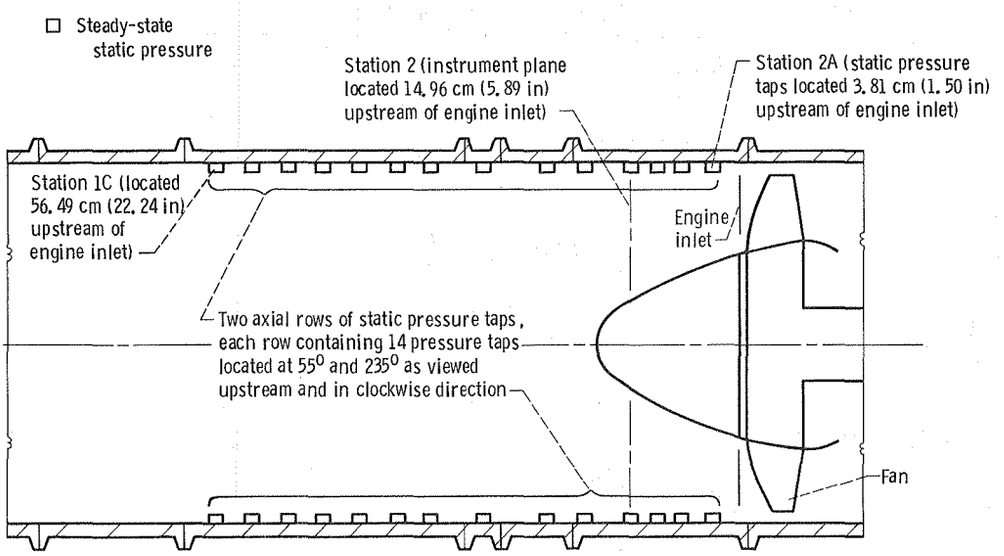

Figure 4. - Inlet duct assembly.

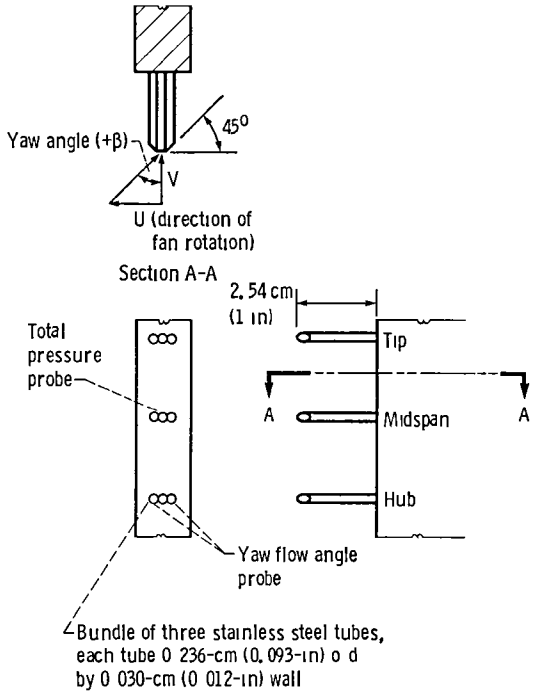

Figure 5 - Station 2 yaw flow angle measurement rake.

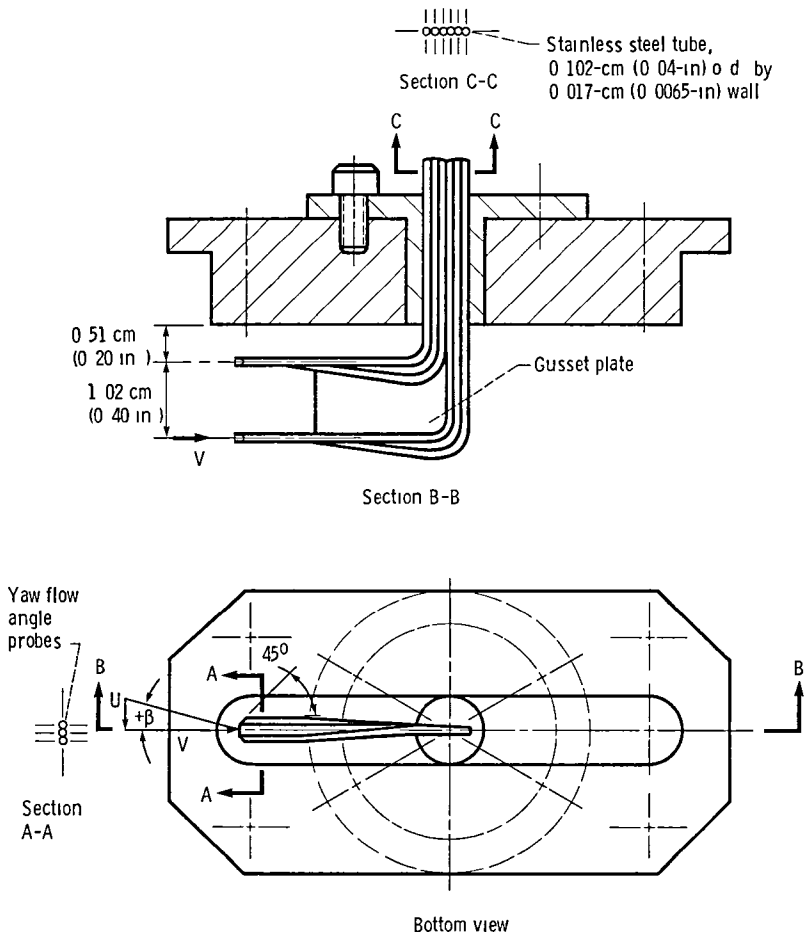

Figure 6 - Tip boundary-layer yaw flow angle probes located at station 2.

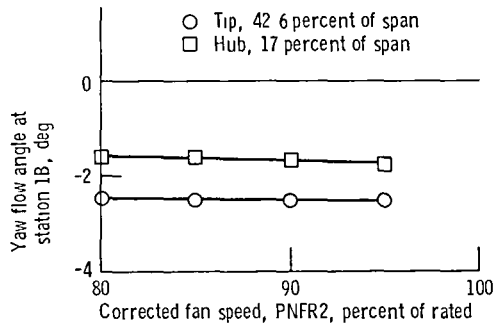

Figure 7 - Yaw flow angle at station 1B as function of corrected fan speed with no pressure and temperature distortion (clean inlet). Reynolds number index, 0 5.

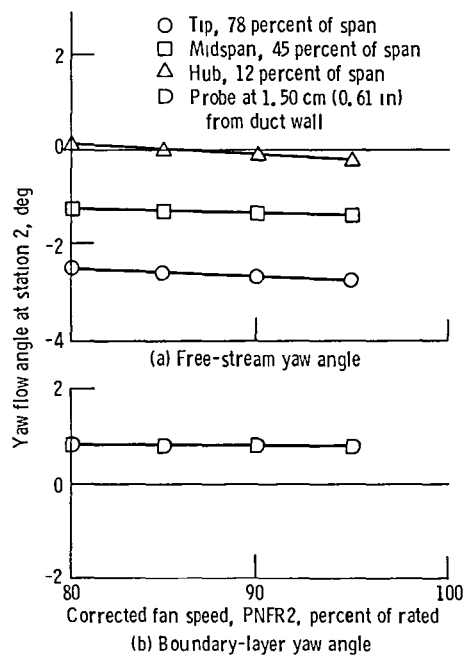

Figure 8. - Yaw flow angle at station 2 as function of corrected fan speed with no pressure and temperature distortion (clean inlet) Reynolds number index, 0.5

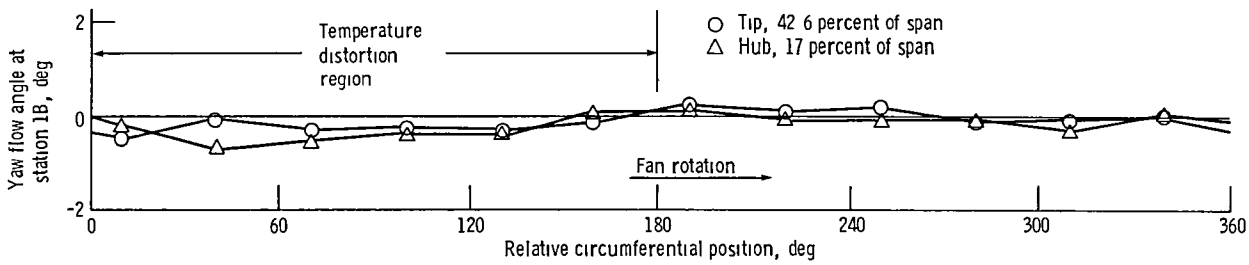

Figure 9 - Yaw flow angle variation at station 1B

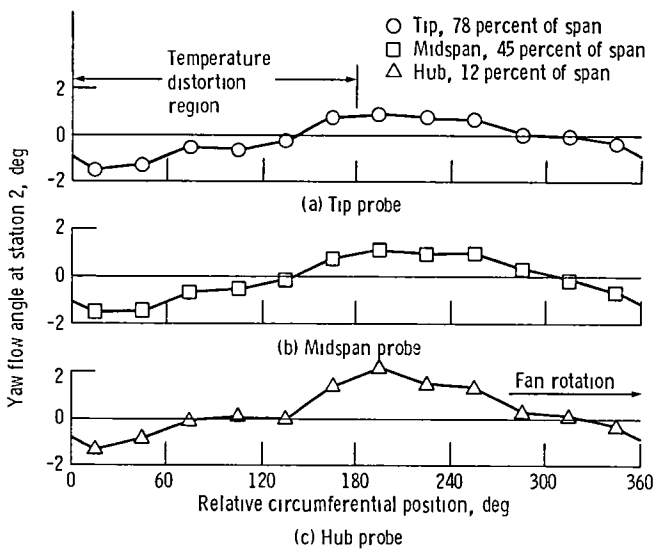

Figure 10 - Yaw flow angle variation at station 2

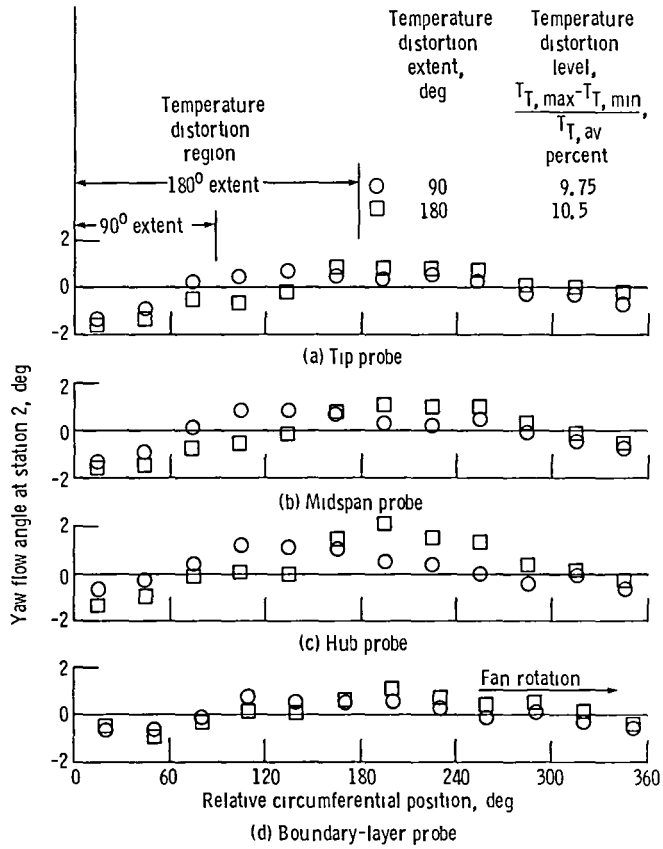

Figure 11 - Effect of distortion extent on yaw flow angle variation at station 2 with Reynolds number index of 0 5

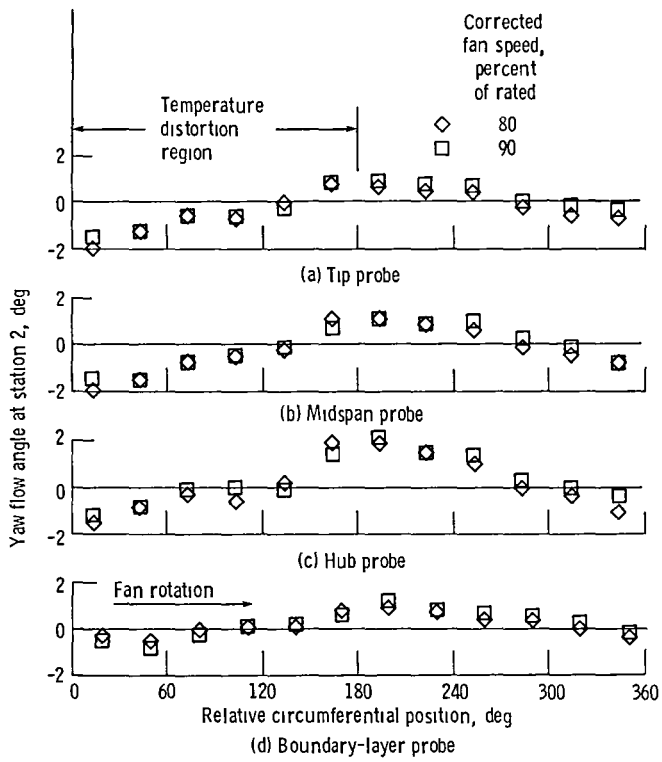

Figure 12 - Effect of corrected fan speed on yaw flow angle variation at station 2

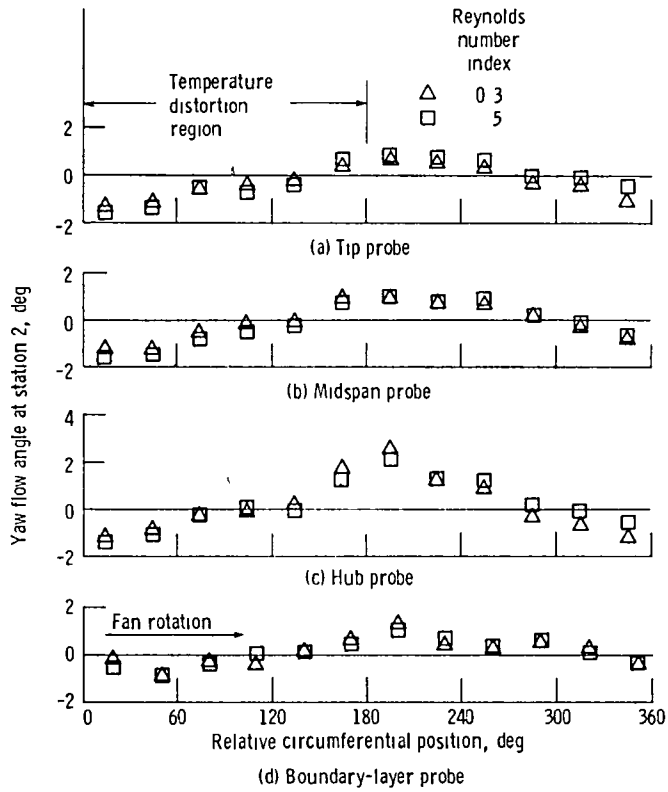

Figure 13 - Effect of Reynolds number index on yaw flow angle variation at station 2 with a corrected fan speed of 90 percent.

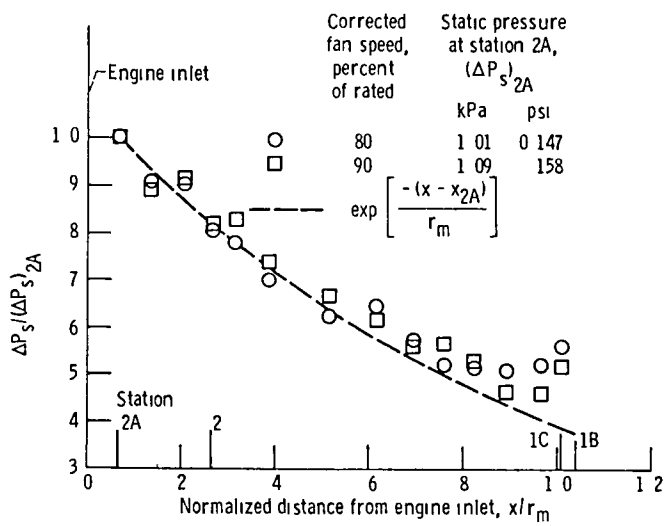

Figure 14 - Effect of corrected fan speed on pressure distortion along inlet duct wall. Temperature distortion, 180° extent and 10 5 percent, Reynolds number index, 0 5

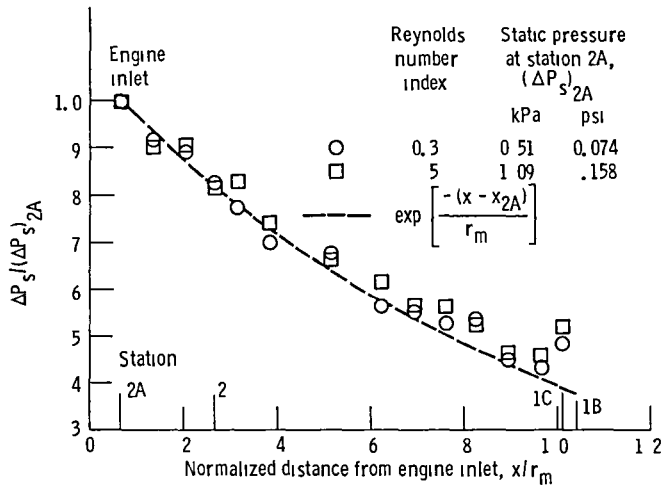

Figure 15 - Effect of Reynolds number index on static pressure distortion along inlet duct wall Temperature distortion, 180° extent and 10.5 percent, corrected fan speed, 90 percent

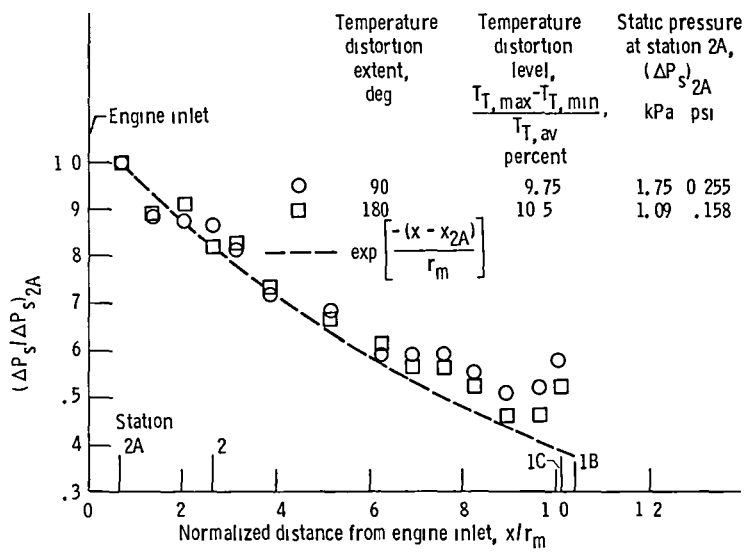

Figure 16 - Effect of temperature distortion extent on static pressure distortion along inlet duct wall Corrected fan speed, 90 percent, Reynolds number index, 0 5

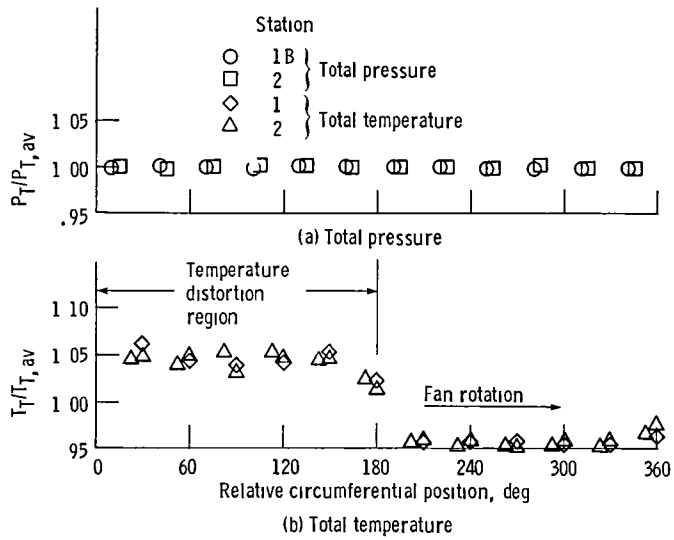

Figure 17 - Circumferential variation of total pressure and total temperature with axial distance along inlet duct.

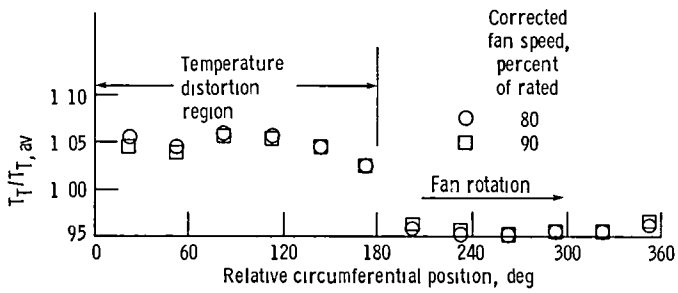

Figure 18 - Effect of corrected fan speed on circumferential total temperature variation at fan inlet (station 2)

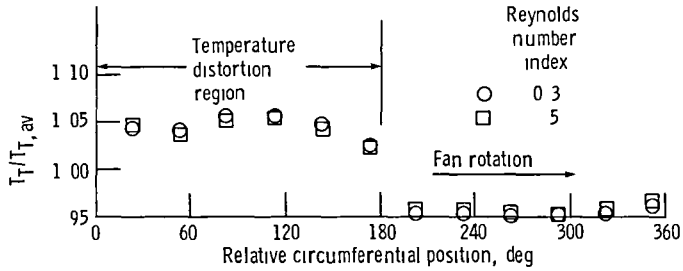

Figure 19 - Effect of Reynolds number index on circumferential total temperature variation at fan inlet (station 2)

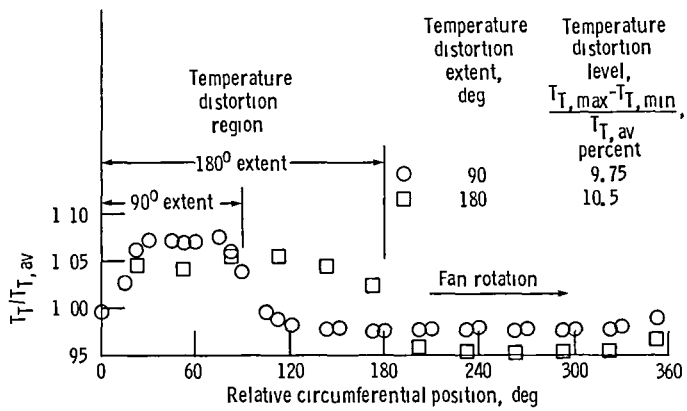

Figure 20. - Effect of distortion extent on circumferential total temperature variation at fan inlet (station 2)

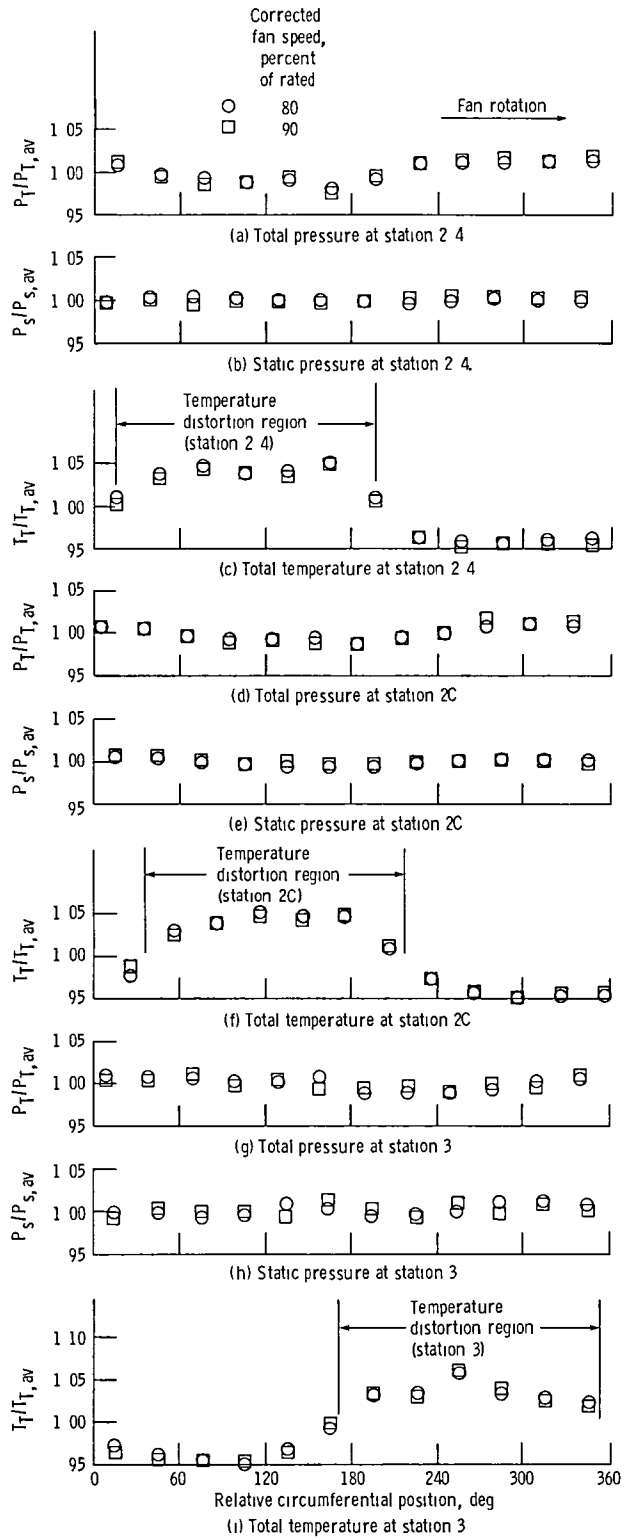

Figure 21 - Effect of corrected fan speed on circumferential total and static pressure and total temperature variation at fan exit, compressor inlet, and compressor exit (stations 2 4, 2C, and 3)

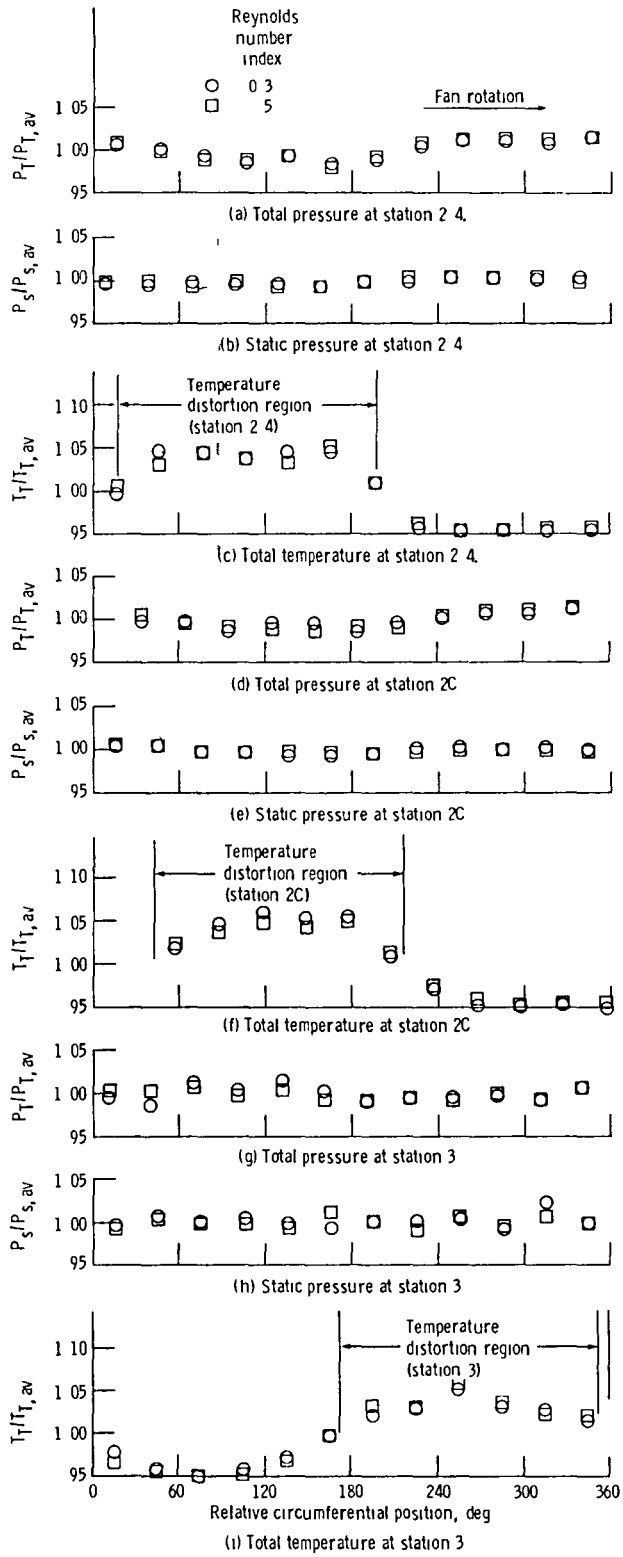

(a) Total pressure at station 2 4.

(b) Static pressure at station 2 4

(c) Total temperature at station 2 4.

(d) Total pressure at station 2C

(e) Static pressure at station 2C

(f) Total temperature at station 2C

(g) Total pressure at station 3

(h) Static pressure at station 3

(i) Total temperature at station 3

Figure 22 - Effect of Reynolds number index on circumferential total and static pressure and total temperature variation at fan exit, compressor inlet, and compressor exit (stations 2 4, 2C, and 3)

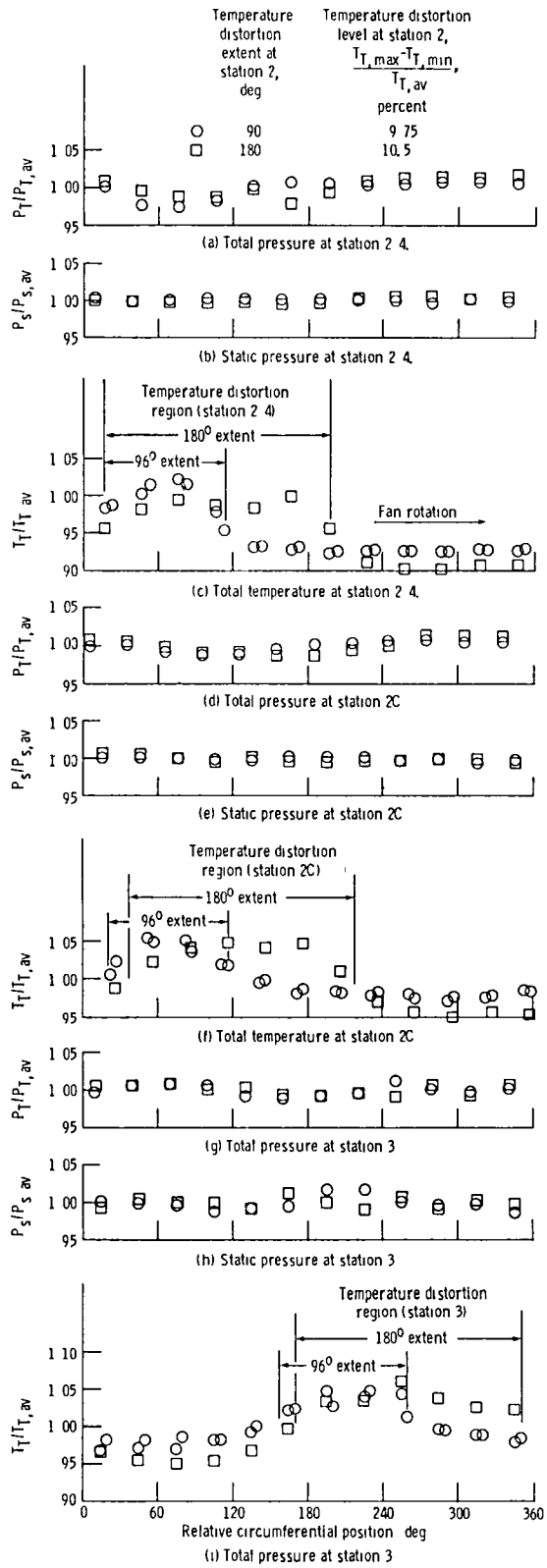

Figure 23 - Effect of temperature distortion extent on circumferential total and static pressure and total temperature variation at fan exit compressor inlet, and compressor exit (stations 2 4, 2C and 3)

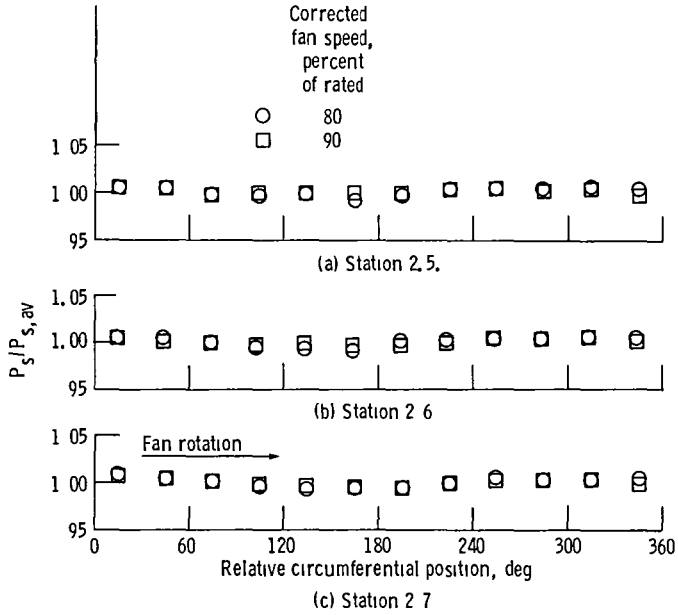

Figure 24. - Effect of corrected fan speed on circumferential static pressure variation at stations 2 5, 2 6, and 2 7 (gooseneck passage upstream of compressor inlet)

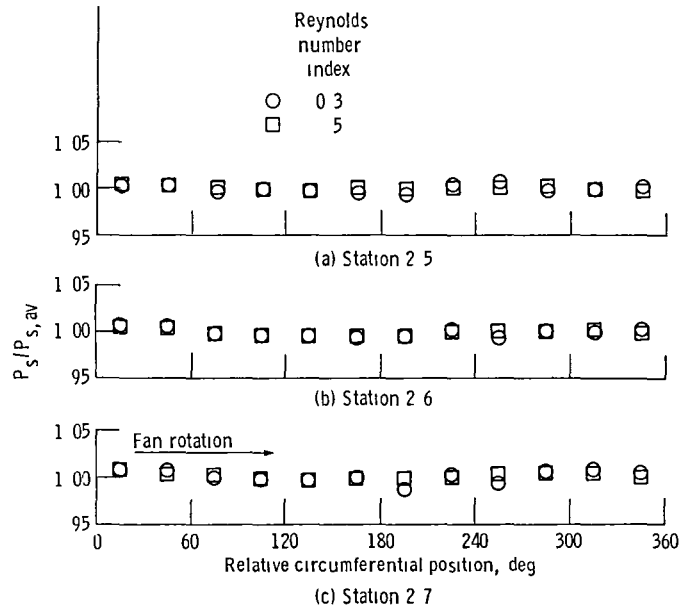

Figure 25 - Effect of Reynolds number index on circumferential static pressure variation at stations 2 5, 2 6, and 2 7 (gooseneck passage upstream of compressor inlet)

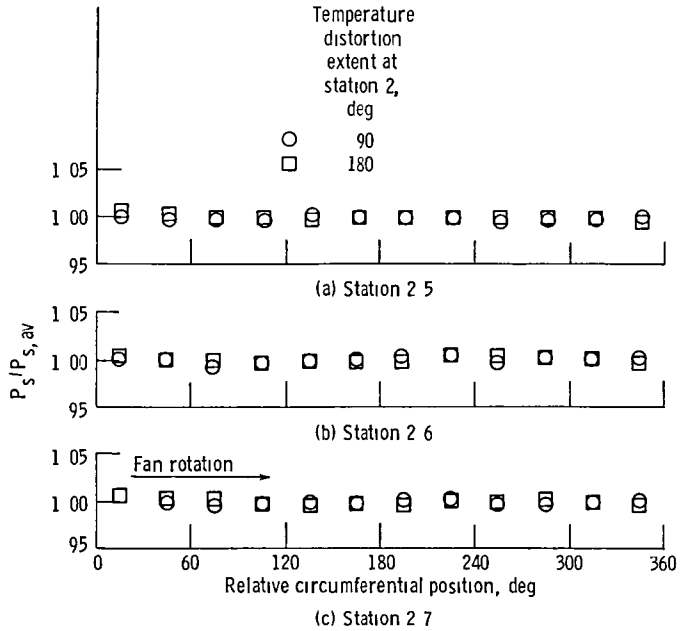

Figure 26 - Effect of temperature distortion extent on circumferential static pressure variation at stations 2 5, 2 6, and 2 7 (gooseneck passage upstream of compressor inlet)

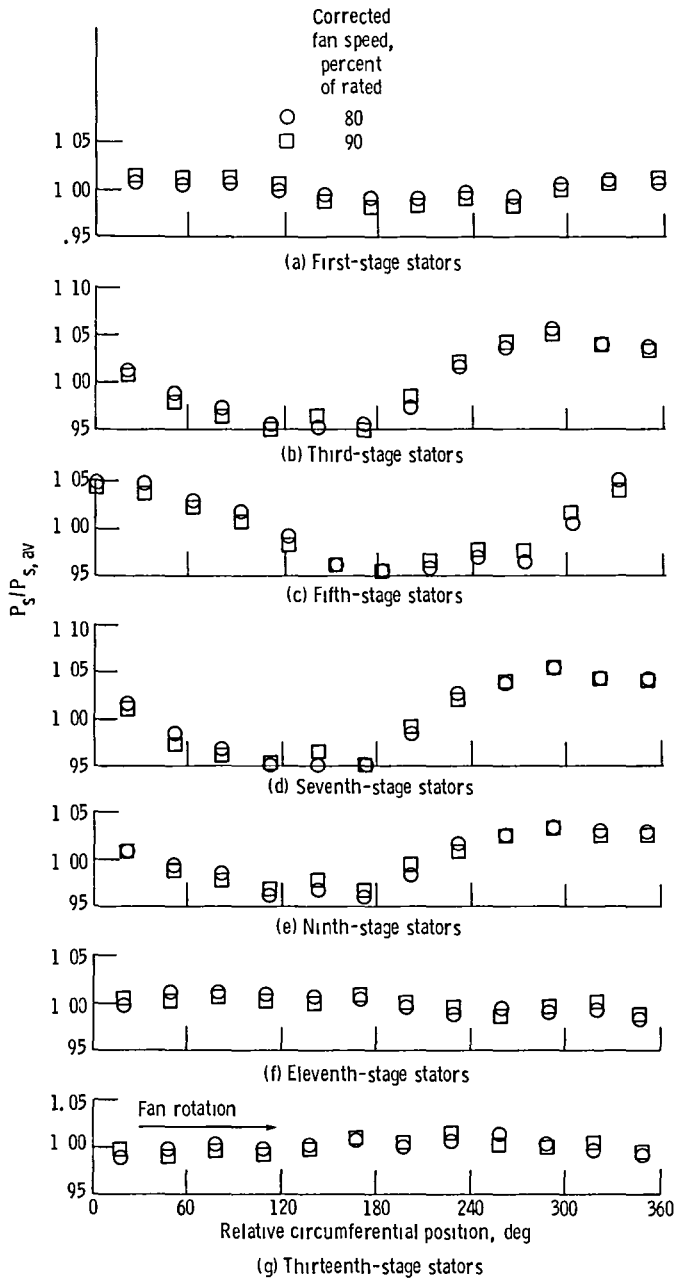

Figure 27 - Effect of corrected fan speed on circumferential static pressure profiles at first- to thirteenth-stage stators (stations 2D to 2R)

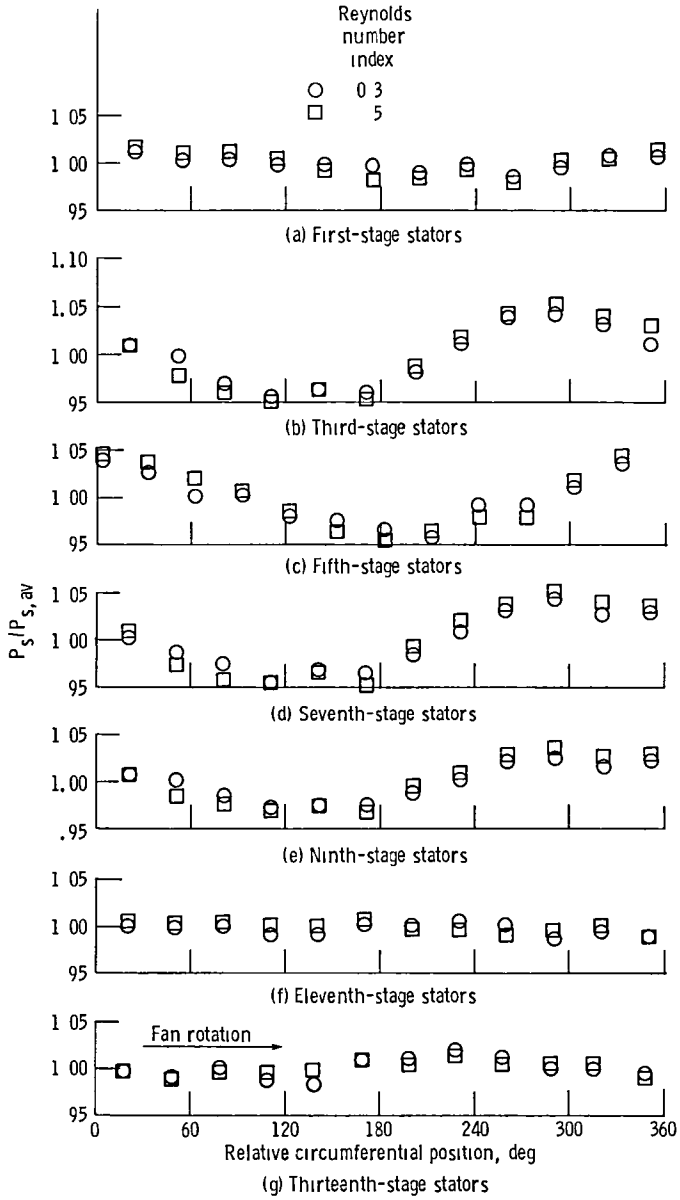

Figure 28. - Effect of Reynolds number index on circumferential static pressure profiles at first- to thirteenth-stage stators (stations 2D to 2R)

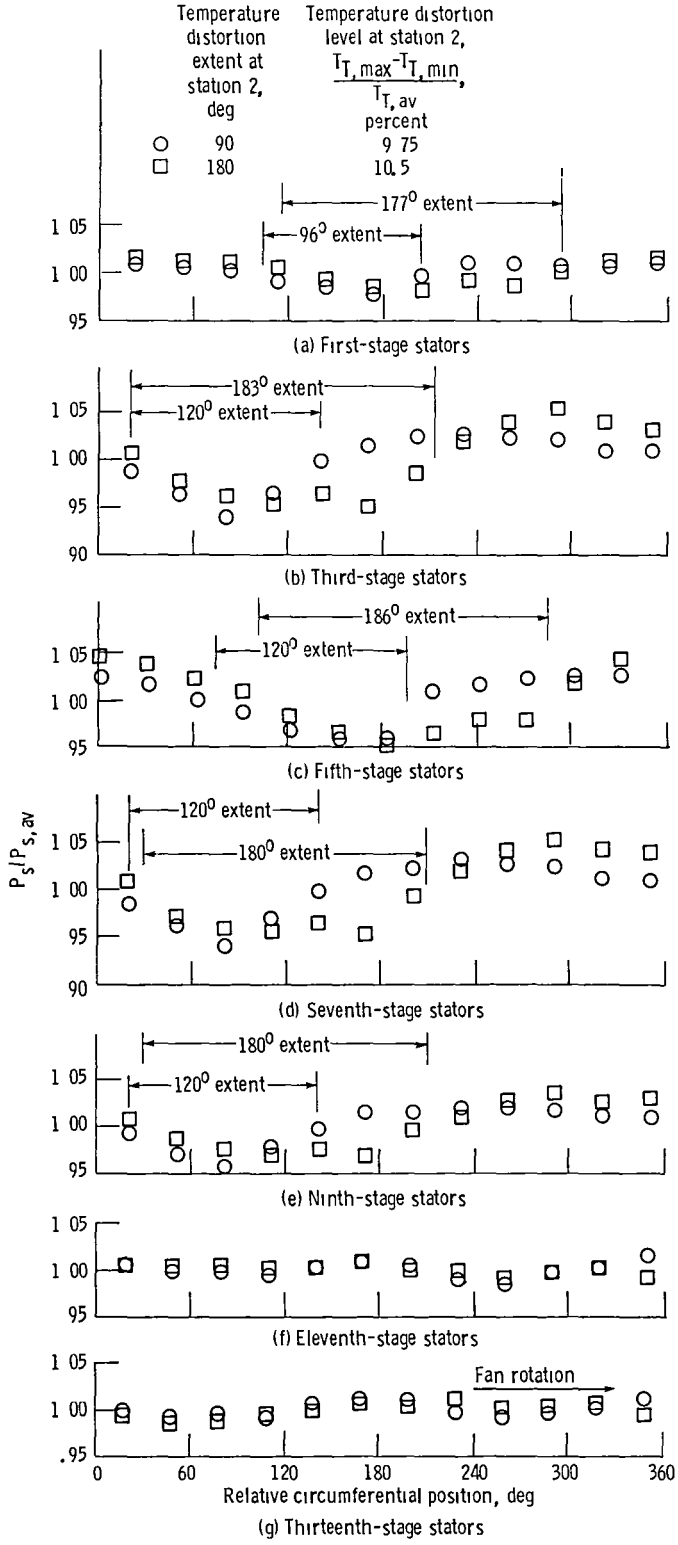

Figure 29 - Effect of temperature distortion extent on circumferential static pressure profiles at first- to thirteenth-stage stators (stations 2D to 2R)

1 Report No	2 Government Accession No	3 Recipient's Catalog No
NASA TM-86896		

4 Title and Subtitle	5 Report Date
Effect of Steady-State Temperature Distortion on Inlet Flow to a High-Bypass-Ratio Turbofan Engine	January 1985
	6 Performing Organization Code: 505-40-74

7 Author(s)	8 Performing Organization Report No
Ronald H. Soeder, Charles M. Mehalic, and Kevin Stancik	E-2369
	10 Work Unit No

9 Performing Organization Name and Address	11 Contract or Grant No
National Aeronautics and Space Administration Lewis Research Center Cleveland, Ohio 44135	
	13 Type of Report and Period Covered: Technical Memorandum

12 Sponsoring Agency Name and Address	14 Sponsoring Agency Code
National Aeronautics and Space Administration Washington, D.C. 20546	

15 Supplementary Notes

Ronald H. Soeder and Charles M. Mehalic, NASA Lewis Research Center; Kevin Stancik, Air Force Systems Command Liaison Office, Lewis Research Center, Cleveland, Ohio.

16 Abstract

The effects of circumferential inlet temperature distortion on the flow characteristics between a distortion generator and a high-bypass-ratio turbofan engine and through its compression system were experimentally evaluated in support of the effort to generate analytical models. The flow characteristics were defined by the inlet duct, the flow angles, and the total temperature, total pressure, and static pressure profiles in the inlet duct and through the fan and compressor. The effects of Reynolds number, rotor speed, and distortion extent were also considered.

17 Key Words (Suggested by Author(s))	18 Distribution Statement
High-bypass-ratio turbofan engine; Inlet flow angle; Inlet and internal total temperature distortion	Unclassified - unlimited STAR Category 07

19 Security Classif (of this report)	20 Security Classif (of this page)	21 No of pages	22 Price*
Unclassified	Unclassified		

*For sale by the National Technical Information Service, Springfield, Virginia 22161

End of Document